ORGANIC PROCESS RESEARCH & DEVELOPMENT
OPR&D
Article
Cite This: Org. Process Res. Dev. 2018, 22, 697−706
pubs.acs.org/OPRD

Cooling Crystallization of Indomethacin: Effect of Supersaturation, Temperature, and Seeding on Polymorphism and Crystal Size Distribution

Chandrakant R. Malwade* and Haiyan Qu

Department of Chemical Engineering, Biotechnology and Environmental Technology, University of Southern Denmark, 5230 Odense M, Denmark

Supporting Information

ABSTRACT: In this work, the effect of crystallization parameters, i.e., supersaturation, seeding, and temperature, on the polymorphism and crystal size of a nonsteroidal anti-inflammatory drug, indomethacin (IMC), was investigated. First, several crystallization solvents (ethanol, methanol, ethyl acetate, acetone, acetonitrile, and dichloromethane) were screened through the measurement of IMC solubility at different temperatures. This was followed by the investigation of IMC nucleation through measurement of induction times in selected solvents at two supersaturations. Finally, seeded cooling crystallization of IMC in ethanol was performed with different process parameters to investigate the influence on the polymorphism and crystal size distribution. Remarkably long induction times were observed for IMC in ethanol and ethyl acetate solutions, while a shorter induction time was observed in acetone. Cooling crystallization of IMC from ethanol confirmed that supersaturation, operating temperature, and seeding do affect the polymorphism as well as crystal size distribution of IMC. Fine needle-shaped crystals of metastable α-IMC were obtained at 5 °C with high supersaturation even in the presence of γ-IMC seeds, while rhombic platelike crystals of thermodynamically stable γ-IMC were obtained in the remaining experiments. The seed loading only marginally influenced the crystal growth rate and median particle diameter. Particle size analysis of the crystals obtained showed a bimodal distribution in all experiments, and a larger median particle diameter was observed at 15 °C with high supersaturation.

1. INTRODUCTION

Most of the processes for manufacturing of active pharmaceutical ingredients (APIs) involve crystallization as a purification technique for the intermediates or APIs. In addition to the unique capability of delivering high-purity crystalline product, the advantage of using crystallization for purification of APIs also includes the ability to engineer final product properties such as polymorphism, crystal size, and shape to the desired level. Although the amorphous form of APIs possesses better dissolution properties, the crystalline form is mostly preferred for the development of various formulations because of the stability issues associated with the amorphous form.[1] The amorphous form of an API is a metastable form and tends to crystallize upon storage, thereby changing its physical properties, leading to changes in bioavailability. However, most of the crystalline APIs exhibit polymorphism, where the API can exist in several crystal forms having different arrangements of molecules in the unit cell. It is a very well established fact that the selection of a suitable polymorph is crucial for the development of drug products, as the polymorphs may have significantly different physicochemical properties (e.g., dissolution rate, solubility) and therefore different bioavailabilities and stabilities. The notorious example of the antiviral drug ritonavir, a batch of which had to be withdrawn from the market because of the appearance of a less soluble polymorph, illustrates the importance of polymorphism in the pharmaceutical industry.[2] Several reports of polymorphs of APIs exhibiting significantly different physical and chemical properties have been mentioned in the literature.[3,4] Similarly, the particle size and shape of APIs are crucial quality attributes that are known to influence downstream processing, formulation processes, and drug product attributes such as rate of drug release, bioavailability, etc.[5,6] Therefore, control of polymorphism and particle size and shape during crystallization of APIs assumes great significance for the pharmaceutical industry. These quality attributes of APIs are often very sensitive to the crystallization process parameters such as method and degree of supersaturation (cooling, evaporation, antisolvent addition, etc.), operating temperature, solvent, impurities, agitation, etc.[3,7−11] Therefore, a thorough understanding of crystallization process parameters and their impact on critical quality attributes of APIs is required in order to produce APIs of consistent and desired quality. The objective of this work is twofold: first, to investigate the interplay between crystallization process parameters and quality attributes of APIs, and second, to understand the mechanisms involved in the crystallization process.

1-(*p*-Chlorobenzoyl)-5-methoxy-2-methylindole-3-acetic acid, also known as indomethacin (IMC), a nonsteroidal anti-inflammatory drug, was selected in this work as a model compound. IMC is known to exhibit five polymorphs and several solvates.[12] However, among the five polymorphs, only α-IMC and γ-IMC are obtained most commonly. These two IMC polymorphs are monotropically related to each other: α-IMC (mp 149−154 °C) is a metastable form, and γ-IMC (mp 158−161 °C) is the thermodynamically most stable form. Distinct crystal packing diagrams of α-IMC and γ-IMC

Received: March 19, 2018
Published: May 25, 2018

DOI: 10.1021/acs.oprd.8b00078
Org. Process Res. Dev. 2018, 22, 697−706

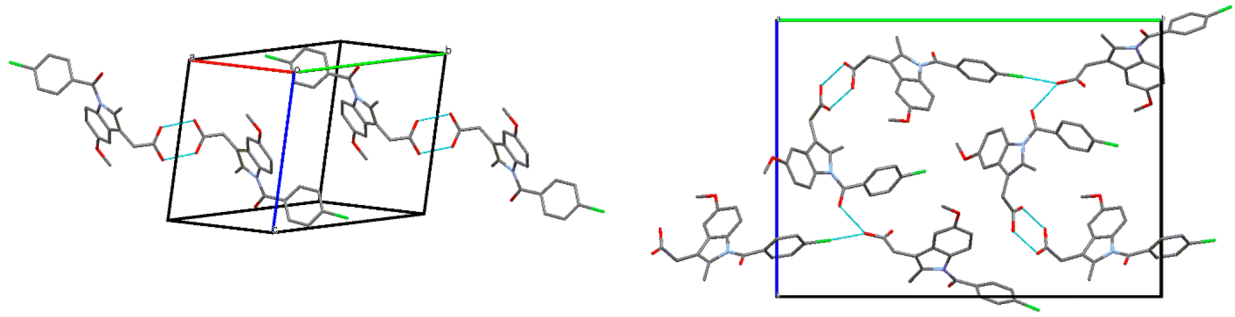

Figure 1. Crystal packing diagrams of (left) γ-IMC and (right) α-IMC.

resulting to their different physical and chemical properties are shown in Figure 1. The asymmetric unit of α-IMC contains three IMC molecules: two molecules hydrogen-bonded through carboxylic acid groups and a third molecule attached to the dimer via a hydrogen bond between its carboxylic acid group and one of the amide carbonyls of the dimer, as shown in Figure 1.[13] On the contrary, γ-IMC has two IMC molecules hydrogen-bonded through carboxylic acid groups. It has also been reported that γ-IMC crystals exist as rhombic plates while α-IMC crystals have a fine short needlelike shape.[14] There are several reports illustrating the differences in physical and chemical properties such as solubility, dissolution rate, reactivity, morphology, and stability of IMC polymorphs.[13−16] Only preliminary crystallization studies of IMC have been carried out previously, which clearly indicate a strong dependence of the polymorphic and morphological outcome on the process parameters.[14,17,18] In the present work, the effect of crystallization process parameters such as solvent, temperature, supersaturation, seeding with γ-IMC, etc. on the polymorphism and particulate properties of IMC is investigated. This work was organized in the following order: First, solvents of varying polarity were screened via measurement of the solubility of IMC at different temperatures. This was followed by characterization of IMC nucleation through measurement of induction times in the selected solvents. Finally, seeded cooling crystallization of IMC was performed from ethanol. Crystallization experiments were performed at different supersaturations, temperatures, and γ-IMC seed loads to induce crystallization. Process analytical technology tools such as an ATR-FTIR probe were employed to monitor desupersaturation.

2. MATERIALS AND METHODS

2.1. Chemicals. Ethanol of TechniSolv grade (purity ≥99.5%) purchased from VWR Chemicals was used in this work. Methanol, acetone, ethyl acetate, acetonitrile, and dichloromethane of CHROMASOLV grade (purity ≥99.9%) obtained from Honeywell Specialty Chemicals were used in this work. IMC of purity ≥99% purchased from Shanghai Hungsun Chemical Co., Ltd. was used after a recrystallization step. Ultrapure MilliQ water obtained from a Purelab Chorus (ELGA) water purifier system was used.

2.2. Characterization of Indomethacin. Recrystallized IMC was analyzed with X-ray powder diffraction (XRPD), and the obtained XRPD patterns were compared with the calculated XRPD patterns of γ-IMC (INDMET01) and α-IMC (INDMET02) obtained from The Cambridge Structural Database (CSD), as shown in Figure 2.[19] α-IMC was produced from recrystallized IMC as per the procedure mentioned by

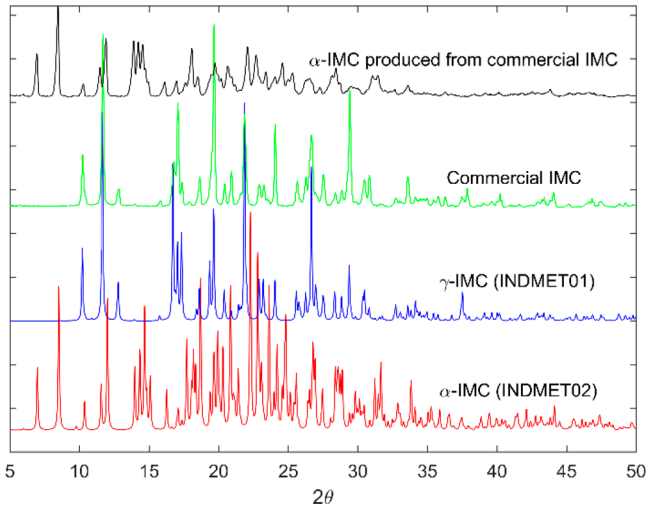

Figure 2. Measured and calculated XRPD patterns of γ-IMC and α-IMC.[19,23]

Kaneniwa et al.,[20] which involved crystallization of IMC from a hot solution in methanol by addition of water as an antisolvent. Comparison of the XRPD patterns of recrystallized IMC and α-IMC produced from it showed very good agreement with the calculated patterns of γ-IMC and α-IMC, respectively. A Rigaku MiniFlex600 benchtop X-ray diffractometer equipped with a Cu Kα radiation source operating at 40 kV and 15 mA, a graphite monochromator, and a NaI scintillation detector was used for analysis of samples. Samples were scanned from 2θ = 5° to 50° with a step size of 0.02° at a speed of 10 deg/min. IMC polymorphs were also characterized by FT-Raman spectroscopy and simultaneous thermal analysis (STA). A Bruker MultiRam FT-Raman spectrometer equipped with a Nd:YAG laser sample excitation source (1064 nm) and a liquid-nitrogen-cooled Ge diode detector was used for analysis. The samples were scanned in the wavenumber range of 3500−500 cm^{-1} with spectral resolution of 4 cm^{-1}. Raman spectra of both IMC polymorphs (provided in the Supporting Information) clearly show the distinct features of α- and γ-IMC and good agreement with the literature data.[21,22] A simultaneous thermal analyzer (STA 449 F3 Jupiter, NETZSCH-Gerätebau GmbH) was used for characterization of IMC polymorphs. The samples were heated from room temperature to 200 °C in an alumina crucible at heating rate of 10 °C/min. Thermograms of IMC polymorphs (provided in the Supporting Information) confirmed the melting points of γ- and α-IMC as 158.6 and 152.4 °C, respectively. It is also obvious that both polymorphs melt cleanly without any degradation and that the thermodynamically stable (γ-IMC) form has a higher melting point than

DOI: 10.1021/acs.oprd.8b00078
Org. Process Res. Dev. 2018, 22, 697−706

the metastable form, thereby confirming their monotropic relationship.

2.3. Experimental Methods. *2.3.1. Solubility Measurement of Indomethacin.* Organic solvents representing the alcohol, ketone, ester, halogenated alkane, and nitrile classes were considered for screening. The classical isothermal technique was used to measure the solubility of γ-IMC in ethanol, methanol, ethyl acetate, acetonitrile, acetone, and dichloromethane. The solubility was measured at 15, 25, 35, and 45 °C, except for dichloromethane, where it was measured up to 35 °C because of the lower boiling point. The procedure for solubility measurement involved preparation of a suspension with an excess amount of solute in 2 mL of solvent contained in a 10 mL glass vial. Sealed vials were maintained at constant temperature under magnetic stirring for 24 h to attain equilibrium. A detailed description of the apparatus used for the measurements is provided by Malwade and Christensen.[24] At the end of the equilibration, the saturated solution was separated from the excess solid phase with a syringe and 0.2 μm PTFE filters, appropriately diluted, and analyzed by high-performance liquid chromatography (HPLC) to determine the concentration of IMC. The solid phase was analyzed by XRPD to ascertain any possible phase change during the solubility measurement. Four repetitions were performed for each measurement. The solubility of α-IMC was measured in ethanol at 15, 25, 35, and 45 °C. However, the transformation of metastable α-IMC into stable γ-IMC during solubility measurement was observed, as reported previously in the literature.[20] Therefore, samples were equilibrated for 2 h to avoid this transformation, which was confirmed by XRPD analysis of the excess solid phase. Thus, the measured solubility of α-IMC can be considered as the kinetic solubility instead of the equilibrium solubility.[25,26]

2.3.2. Induction Time Measurement of Indomethacin. The nucleation behavior of IMC in ethanol, acetone, and ethyl acetate was determined through the measurement of induction times. An EasyMax102 workstation (Mettler-Toledo AutoChem) equipped with two 100 mL reactors, an overhead stirrer, and a solid-state thermostat enabled cooling/heating jacket (Figure 3) was used to measure the induction times of IMC. Nucleation of IMC was detected by monitoring the turbidity of the solution with a Crystal Eyes turbidity probe (HEL Group, Borehamwood, U.K.). A ReactIR 15 ATR-FTIR probe (Mettler-Toledo AutoChem) equipped with an AgX probe interface (6 mm × 1.5 m fiber), a DiComp (Diamond) probe tip, and a liquid-nitrogen-cooled MCT detector was also used to detect nucleation of IMC in solution. The induction time of IMC was measured in ethanol, acetone, and ethyl acetate at two temperatures (5 and 15 °C), as shown in Table 1. The corresponding supersaturations ($S = c/c^*$, where c and c^* are the starting and equilibrium concentrations of γ-IMC, respectively) at the studied temperatures are also shown in Table 1. Three repetitions were performed for each measurement. The procedure included preparation of 100 mL solutions of IMC with the specified initial concentrations in the respective solvents shown in Table 1 and cooling to the target temperature at 10 °C/min under constant stirring at 300 rpm. Saturated solutions of IMC in ethanol and ethyl acetate were prepared at 45 °C, while the solution in acetone was prepared at 35 °C because of the lower boiling point of acetone. Before being cooled to the target temperature, the solutions were heated 5 °C above the saturation temperature in order to obtain a clear solution. The time from when the thorough dissolution reached the target temperature until the appearance of detectable nuclei was considered as the induction time.

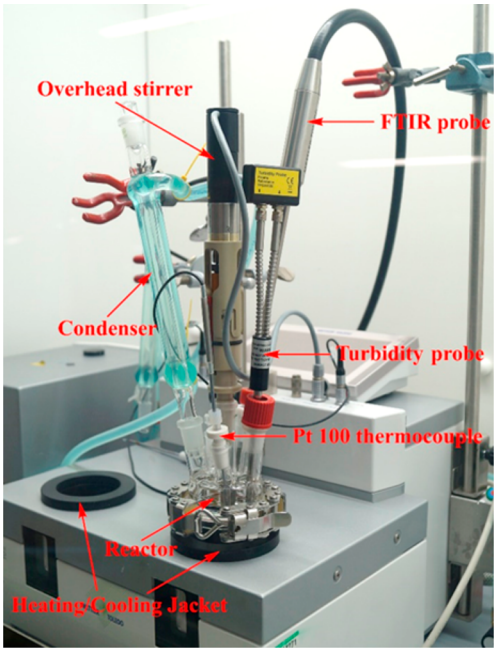

Figure 3. Experimental setup used for induction time and crystallization experiments.

Table 1. Experimental Plan and Operating Parameters for Induction Time Measurements

solvent	scale (mL)	stirring speed (rpm)	initial concentration (g/100 g of solvent)	temperature (S^a)
ethanol	100	300	5.1	5 °C (4)
			6.4	15 °C (3.2)
acetone	100	300	16.5	5 °C (3)
			16.5	15 °C (1.8)
ethyl acetate	100	300	6.5	5 °C (2.3)
			6.5	15 °C (1.7)

[a] S is the supersaturation, calculated as the ratio of the initial concentration to the equilibrium concentration of γ-IMC.

2.3.3. Crystallization of Indomethacin. Crystallization of IMC was performed by preparing a solution with certain concentration at a high temperature and then cooling the solution to the studied temperature (5 or 15 °C). The experimental plan is shown in Table 2. For each temperature, two supersaturations were used, as shown in Table 2. In order to induce crystallization of IMC, cooling crystallization experiments were seeded with γ-IMC. Seed loads equivalent to 1, 2, and 4% of the difference between the starting and equilibrium concentrations (ΔC) were used for each supersaturation. Seeds of γ-IMC were prepared by recrystallization of IMC from acetonitrile and consisted of a sieve fraction of range 71−125 μm. The concentration of IMC during seeded cooling crystallization was monitored with an ATR-FTIR probe. The procedure included preparation of a fixed-concentration solution of IMC in ethanol in an EasyMax reactor and maintaining the temperature at 45 °C to ensure complete dissolution of the solute. The solution was then cooled to the target temperature at 10 °C/min, and dry seeds of γ-IMC were added to the solution 10 min after the temperature reached the target value. A constant overhead stirrer speed of 300 rpm was maintained throughout the experiments. IMC crystals obtained

DOI: 10.1021/acs.oprd.8b00078
Org. Process Res. Dev. 2018, 22, 697−706

Table 2. Experimental Plan and Operating Parameters for Crystallization of IMC from Ethanol

experiment no.	temperature (°C)	initial concentration (g/100 g of solvent)	S	seed loading (%)
1	5	3.5	2.65	1
2				2
3				4
4		6.0	4.8	1
5				2
6				4
7	15	3.5	1.75	1
8				2
9				4
10		5.5	2.75	1
11				2
12				4

at the end of the experiment were dried and analyzed by XRPD as well as a particle size analyzer (LS 13 320 laser diffraction particle size analyzer, Beckman Coulter, Inc.) to determine the polymorph and crystal size distribution, respectively.

2.3.4. Calibration of the ATR-FTIR Probe. The concentration of IMC during the crystallization experiments was monitored online using an ATR-FTIR probe. For this purpose, the ATR-FTIR probe was calibrated with different concentrations of IMC in ethanol at 5 and 15 °C. A constant-temperature approach was used, in which an IMC solution of a known concentration was successively diluted by addition of a known amount of ethanol at constant temperature.[27,28] The background scan in air was collected at room temperature before the start of the calibration process. Air was chosen over the pure solvent as a background because of the high sensitivity of IR spectra of solvents to temperature variations. The spectra were collected in the wavenumber range of 3000−650 cm^{-1} with a resolution of 8 cm^{-1}. Each spectrum consisted of 256 scans. Two separate multivariate partial least-squares (PLS) calibration models were developed from 22 FTIR spectra of IMC solutions of varying concentration at 5 and 15 °C using iC IR software (Mettler-Toledo AutoChem). Among the collected spectra during calibration, 70% were used as a training set, while the remainder were used as a test set. The model was constructed by selecting the 1750−1650 cm^{-1} spectral region containing the signals from stretching of the carboxyl and benzoyl carbonyl (>C═O) groups in IMC.[17] Before their use in the calibration model, the spectra were baseline-corrected using cubic spline interpolation, which subtracts a polynomial fitted to the points selected on the baseline from the original spectrum.

3. RESULTS AND DISCUSSION

3.1. Solvent Screening through Solubility of Indomethacin. The solubilities of γ-IMC measured in ethanol, methanol, acetonitrile, acetone, and dichloromethane are shown in Figure 4. The solubility values at 5 °C are extrapolated from the regression model fitted to the experimental data. It is obvious from the figure that the solubility of γ-IMC is highest in acetone, while the lowest solubility was observed in acetonitrile. Moreover, linear behavior of the IMC solubility with respect to temperature was observed in all of the solvents except ethanol and methanol, where an exponential dependence on temperature was observed. The solubility values for IMC in ethanol and

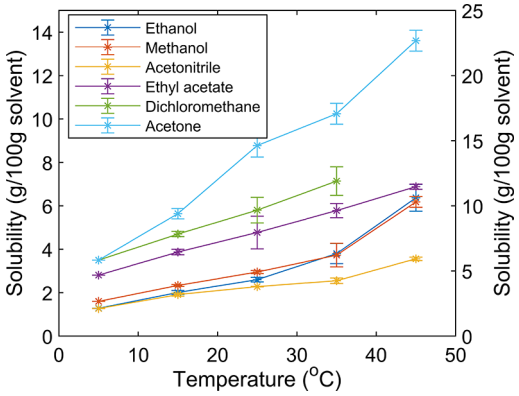

Figure 4. Solubilities of γ-IMC in different solvents. The right ordinate represents the solubility of γ-IMC in acetone. Solid lines are drawn for visual guidance.

methanol were almost the same. The product yield in cooling crystallization strongly depends on the slope of the solubility curve; a larger slope is always desirable in order to obtain higher yields. In the case of acetonitrile, the slope of the IMC solubility curve is not very significant, meaning that the product yield of a cooling crystallization would be rather low. The measured solubility values of IMC correspond very well with previously reported solubility data.[29] XRPD analysis of excess IMC recovered after the solubility measurements confirmed the formation of solvates in acetone, methanol, and dichloromethane at all temperatures, while no phase change was observed in the other solvents. The XRPD patterns from analysis of the solid phase during solubility measurements are provided in the Supporting Information. The solvents ethanol, acetone, and ethyl acetate were considered for further investigation of the nucleation behavior on the basis of the solubility values.

The solubility of metastable α-IMC in ethanol was also measured. The measured solubility of α-IMC is shown in Figure 5 along with the solubility of thermodynamically stable

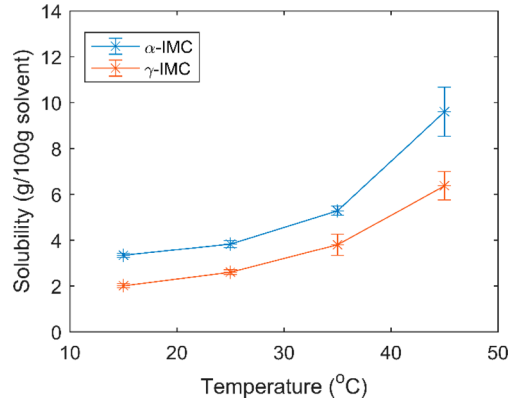

Figure 5. Solubilities of α- and γ-IMC in ethanol at different temperatures.

γ-IMC. During the solubility measurement, the solvent-mediated transformation of α-IMC into γ-IMC was observed, in agreement with previous reports.[20] It was also found that the rate of this transformation increased with increasing temperature, and the transformation was complete in 18 h at 25 °C. Therefore, the solubility samples were agitated for only 2 h to avoid this transformation. It is clear from Figure 5 that the

DOI: 10.1021/acs.oprd.8b00078
Org. Process Res. Dev. 2018, 22, 697−706

kinetic solubility of α-IMC is higher than the solubility of γ-IMC at all temperatures, thereby confirming that the two polymorphs of IMC are monotropically related to each other.

3.2. Induction Time of Indomethacin. Exemplary results from induction time measurements of IMC in ethanol at 5 °C (supersaturation (S) = 4), including temperature, turbidity, and the IMC concentration profile measured with the ATR-FTIR probe, are shown in Figure 6. It is evident that the

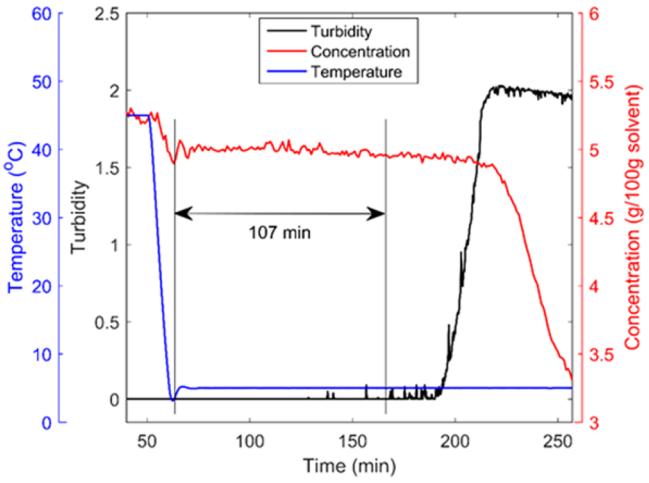

Figure 6. Results of induction time measurements of IMC in ethanol at 5 °C.

supersaturation was generated by rapid cooling of the IMC solution from 45 to 5 °C and maintained at 5 °C until nucleation. The turbidity and IMC concentration of the supersaturated solution were constant until nucleation of IMC happened at 168 min, as indicated by the arrow in Figure 6. The detection of nuclei formed was also confirmed by visual inspection. Upon nucleation of IMC at 168 min, the turbidity of solution started increasing and the IMC concentration started decreasing marginally until 190 min, indicating a slower primary nucleation rate. However, the respective increase and decrease in turbidity and IMC concentration appeared to be faster after 190 min, which might be due to the inducement of secondary nucleation, growth of primary nuclei, or a combination of the two. A large clump consisting of fine needle-shaped crystals was obtained at the end of the experiment. Analysis of these crystals with XRPD, FT-Raman spectroscopy, and STA confirmed crystallization of metastable α-IMC. Exemplary results from induction time measurements of IMC in acetone at 15 °C (S = 1.81) are shown in Figure 7. It is evident from the concentration and turbidity profiles that the nucleation of IMC occurred 17 min after the solution was cooled to 15 °C. Thus, a relatively shorter induction time of IMC was observed in acetone. Moreover, the nucleation kinetics appears to be very fast from the sharp increase in turbidity and decrease in IMC concentration. A dense slurry of fine needle-shaped crystals was obtained at the end of experiment. The crystals were analyzed with XRPD and STA. The XRPD patterns clearly showed additional peaks compared with α- and γ-IMC, indicating the formation of an acetone solvate. STA analysis of the crystals confirmed the formation of a nonstoichiometric acetone solvate. The thermogram of crystals clearly showed an endothermic peak corresponding to the desolvation of acetone at 85.7 °C, followed by crystallization of a mixture of α- and γ-IMC, as is evident

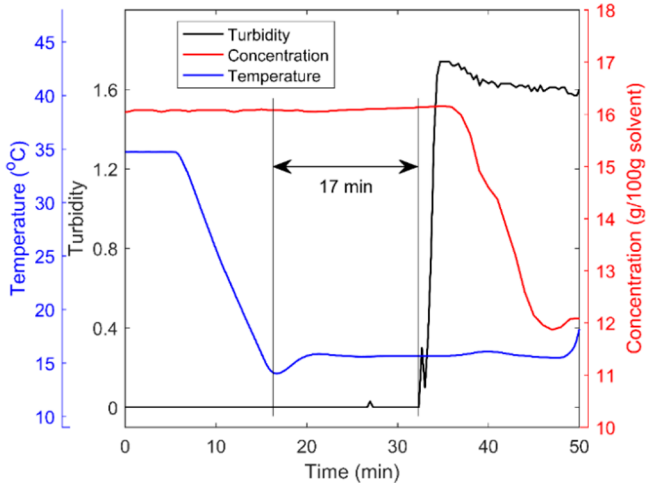

Figure 7. Results of induction time measurements of IMC in acetone at 15 °C.

from the two exothermic peaks corresponding to their melting temperatures. In the case of ethyl acetate, no nucleation of IMC was observed even after waiting for 5 h for both supersaturations used during the induction time measurements. Table 3 summarizes the average results of the IMC induction time measurements from all of the experiments. As expected, an increase in induction time of IMC in ethanol and acetone is observed with a decrease in driving force (i.e., supersaturation). The stochastic nature of nucleation is also evident from the different induction times obtained in the repeated experiments. The longer induction time of IMC in ethanol conforms to the previously reported results,[17] where it has been attributed to the strong hydrogen bonding between IMC and ethanol molecules, which imposed a higher energy barrier for nucleation. Possible solute−solvent interactions are discussed below in order to justify the nucleation behaviors of IMC in ethanol, acetone, and ethyl acetate.

Solute−Solvent Interactions. As described by Davey et al.,[30] a nucleation process can be considered as a two-step process in which the solute molecules preassemble themselves into clusters with a structure that is similar to the prospective crystal form, followed by the growth of this assembly. For this to happen in a crystallization from solution, first the non-covalent interactions between solvent and solute molecules (hydrogen bonding, van der Waals forces, $\pi-\pi$ interactions, etc.) must be broken, which may require varying amounts of energy depending upon the strength of such interactions.[31,32] The strength of such interactions reportedly varies with different solvents.[33] Several other studies describe the importance of non-covalent solute−solvent interactions in influencing the outcome of crystallization processes.[34−39] In the case of IMC nucleation, specifically α-IMC, three hydrogen-bonded molecules of IMC need to orient to form an asymmetric unit with the crystal structure shown in Figure 1. The IMC molecule, with hydrogen-bond acceptor and donor counts of 4 and 1, respectively, has a strong tendency to form intramolecular as well as intermolecular hydrogen bonds. An ethanol molecule, with one hydrogen-bond donor and one acceptor, has the ability to engage all of the hydrogen-bond acceptors as well as the donor of the IMC molecule, as shown in Figure 8. Thus, ethanol−IMC hydrogen-bonding interactions in solution offer a barrier for self-assembly of IMC molecules to form crystal nuclei, which might be the reason for

DOI: 10.1021/acs.oprd.8b00078
Org. Process Res. Dev. 2018, 22, 697−706

Table 3. Results of Induction Time Measurements of IMC in All Solvents

		induction time (min)		solid form	
solvent	no. of repetitions	5 °C	15 °C	5 °C	15 °C
ethanol	3	108 ± 10.6	161 ± 10.26	α-IMC	α-IMC
acetone	4	4.50 ± 4.09	14.0 ± 3.60	solvate	solvate
ethyl acetate	3	–	–	–	–

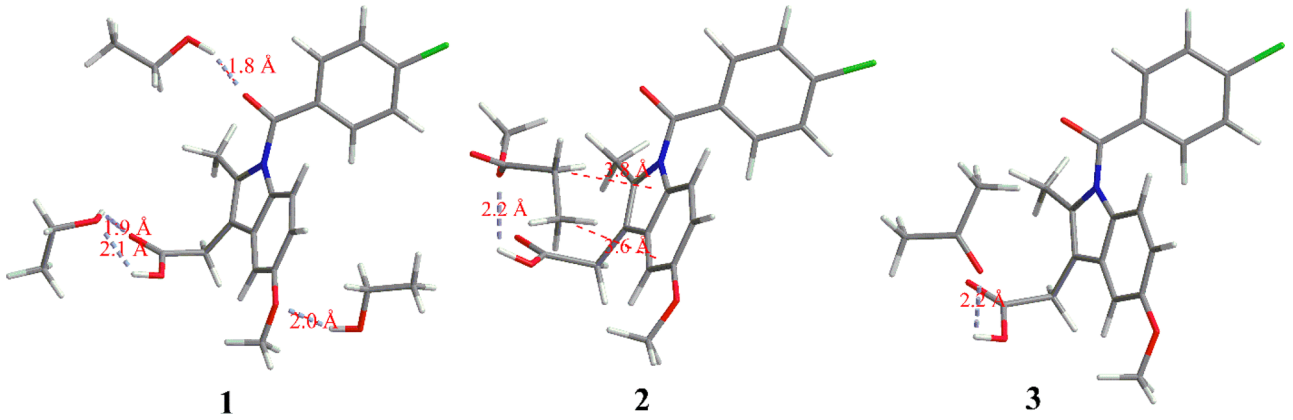

Figure 8. Possible solute−solvent interactions between (1) IMC and ethanol, (2) IMC and ethyl acetate, and (3) IMC and acetone.

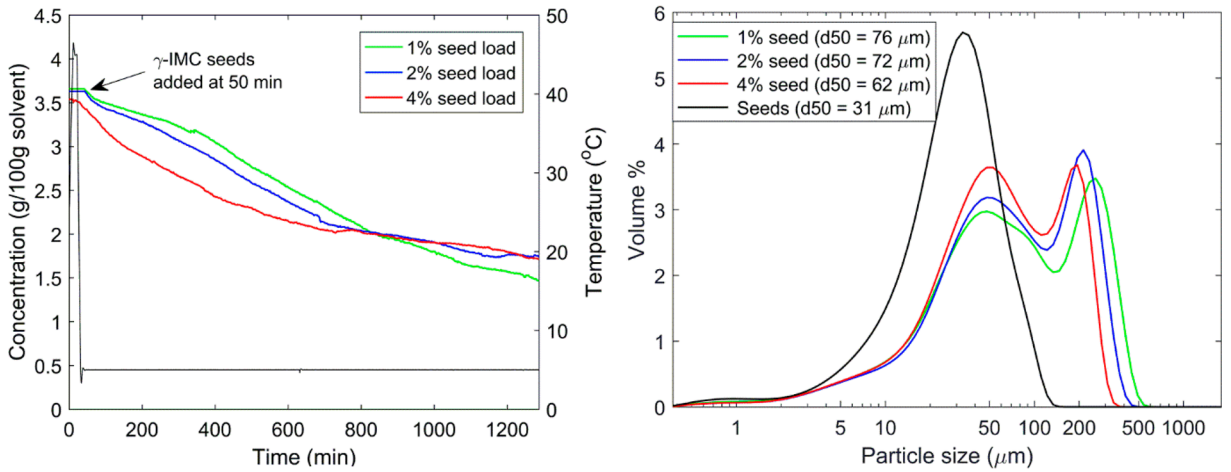

Figure 9. (left) Results of seeded cooling crystallization of IMC from ethanol at 5 °C and low supersaturation. (right) Particle size distributions of the obtained crystals (right).

the remarkably longer induction times of IMC in ethanol. Ethyl acetate, with two hydrogen-bond acceptors, is capable of forming a hydrogen bond only with the carboxylic group of IMC, as shown in Figure 8; however, it has been reported to interact with the π system of the indole ring.[38] Additionally, it is also capable of forming C−H···π interactions with the benzoyl chloride π system through the ethyl group of the ester.[40] These ethyl acetate−IMC interactions might hinder the assembly of IMC molecules to form preassemblies leading to the formation of crystal nuclei. Hydrogen bonding of the acetone molecule with the carboxyl group of the IMC molecule is also shown in Figure 8. Despite the possibility of forming hydrogen-bonded dimers with IMC, very short induction times of IMC were observed in acetone. In this case, intramolecular (IMC−IMC) non-covalent interactions might dominate because of the relatively high concentration of IMC in acetone solution (Figure 7), leading to faster nucleation of the IMC−acetone solvate.

3.3. Crystallization of IMC from Ethanol. *3.3.1. Effect of Supersaturation and Seeding at 5 °C.* Desupersaturation profiles from seeded cooling crystallization of IMC from ethanol at low supersaturation (S = 2.65) and particle size distributions of the obtained products are shown in Figure 9. It is evident from the figure that the IMC concentration starts decreasing after addition of γ-IMC seeds at 50 min, indicating the consumption of supersaturation for the growth of seed crystals or secondary nucleation. The desupersaturation profiles for all seed loadings clearly show very slow consumption of the supersaturation, indicating the slow crystal growth or nucleation rate. XRPD analysis of the crystals obtained at the end of experiment confirmed the polymorph as γ-IMC.

Moreover, the effect of the seed mass on the rate of supersaturation consumption is clearly visible from the desupersaturation profiles and shows that the increase in seed mass (increase in surface area) slightly increases the supersaturation consumption rate. The particle size analysis of the crystals obtained for all seed loadings showed a bimodal

DOI: 10.1021/acs.oprd.8b00078
Org. Process Res. Dev. 2018, 22, 697−706

distribution (Figure 9, right). The median diameter (d_{50}) of the crystals decreases slightly with increasing seed mass. In order to gain insight into the crystal morphology, the obtained crystals were analyzed by scanning electron microscopy (SEM). The SEM image of the crystals obtained for a seed loading of 1%, shown in Figure 10, clearly indicates the rhombic platelike

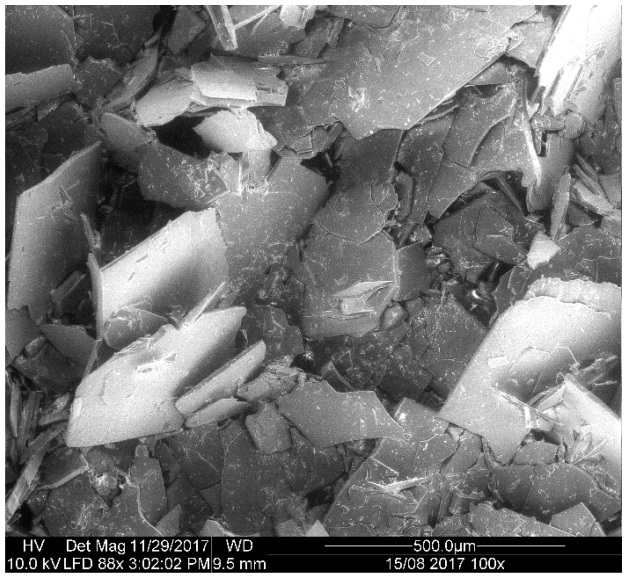

Figure 10. SEM image of γ-IMC crystals obtained in an experiment with a seed loading of 1%.

morphology of γ-IMC. Furthermore, it also shows the smaller particles that might be the fragments of larger plates, as the platelike crystals are more prone to breakage. However, the presence of seed crystals in the solution may induce secondary nucleation as well. Therefore, the bimodal particle size distribution obtained during the experiments can be attributed to the growth of seed crystals and either secondary nucleation, breakage, or a combination of the two.

The results of seeded cooling crystallization of IMC from ethanol at high supersaturation (S = 4.8), including desupersaturation profiles and an SEM image of crystals obtained for 1% seed loading, are shown in Figure 11. Similar to the experiments at low supersaturation, the IMC concentration started decreasing after addition of seeds at 80 min, as shown in the desupersaturation profiles. However, 20–30 min after the addition of seeds, a sudden crystallization of IMC was observed, as is apparent from the sharp decrease in the IMC concentration. A dense slurry of IMC crystals was collected, dried, and analyzed with XRPD and SEM. The SEM image of the crystals shown in Figure 11 (right) confirms the morphology of crystals as fine, short needles. XRPD analysis confirmed the polymorph of obtained crystals as metastable α-IMC despite seeding the experiment with stable γ-IMC. Similar observation was made in our previous work for the crystallization of nitrofurantone from an acetone–water solution, where seeding the supersaturated solution with the polymorphic form I of nitrofurantone monohydrate could not produce form I, but instead, the polymorphic form II was crystallized.[41] According to Desiraju,[39] the crystallization of polymorphs in such situations may follow a kinetically favored path, which can be achieved relatively faster because of the lower activation barrier leading to the crystallization of the metastable form.

3.3.2. Effect of Supersaturation and Seeding at 15 °C. Desupersaturation profiles for seeded cooling crystallization experiments at 15 °C with low and high supersaturation followed similar trends as shown earlier for 5 °C, i.e., slow consumption of supersaturation after addition of seeds and a marginal increase in the rate with increasing seed mass. However, thermodynamically more stable γ-IMC was obtained in all of the experiments at 15 °C. The particle size distributions of crystals obtained at low supersaturation (left) and high supersaturation (right) at 15 °C are shown Figure 12. A nearly unimodal distribution of γ-IMC crystals resulting from the growth of seed crystals was obtained at low supersaturation. Moreover, the effect of the seed mass on the mean diameter seems to be negligible. On the contrary, a bimodal distribution of γ-IMC crystals resulting from growth of seed crystals and either breakage, secondary nucleation, or a combination of the two was obtained at high supersaturation. The effect of seed mass is not very significant at low supersaturation; however, a

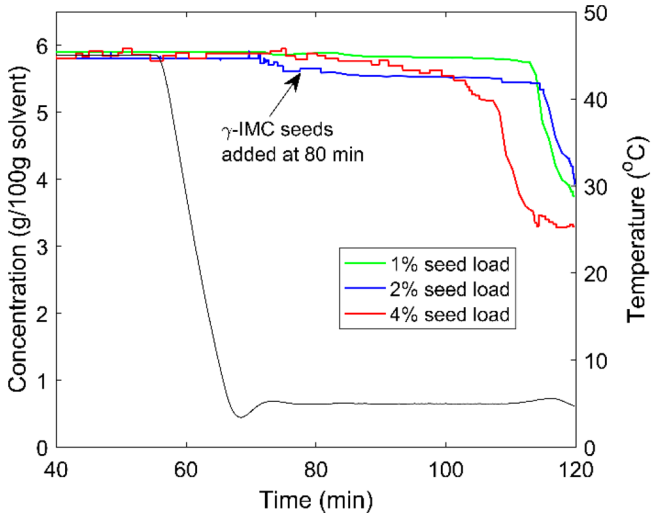

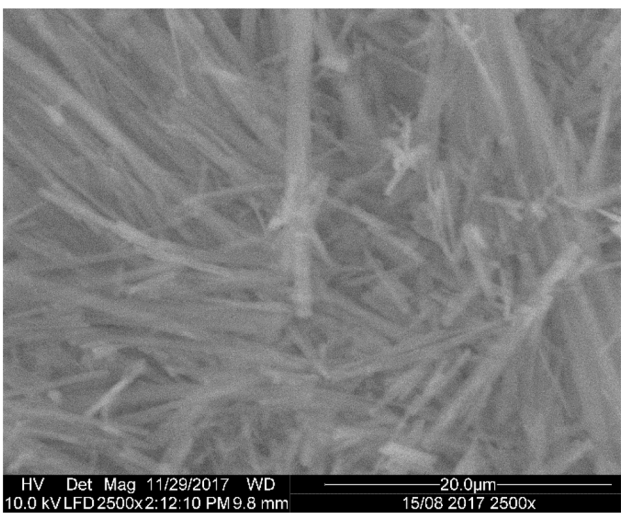

Figure 11. (left) Results of seeded cooling crystallization of IMC from ethanol at 5 °C and high supersaturation. (right) SEM image of crystals obtained with a seed loading of 1%.

DOI: 10.1021/acs.oprd.8b00078
Org. Process Res. Dev. 2018, 22, 697–706

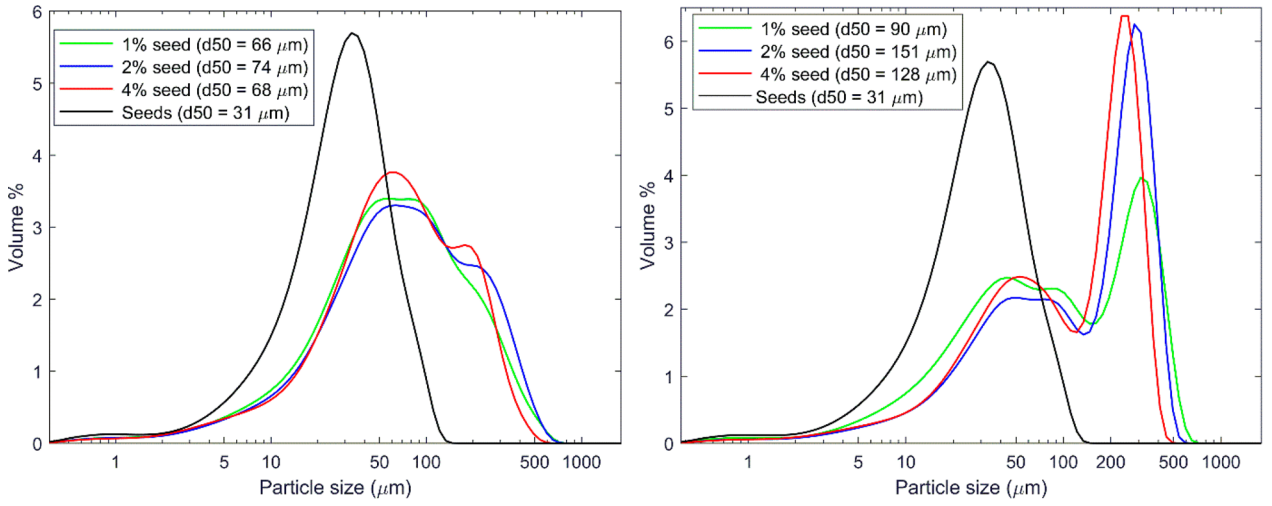

Figure 12. Particle size distributions of γ-IMC obtained at (left) low supersaturation and (right) high supersaturation at 15 °C.

Table 4. Summary of Results of Seeded Cooling Crystallization of IMC in Ethanol

	5 °C						15 °C					
	low *S* (2.65)			high *S* (4.8)			low *S* (1.75)			high *S* (2.75)		
property	1%	2%	4%	1%	2%	4%	1%	2%	4%	1%	2%	4%
polymorph	γ	γ	γ	α	α	α	γ	γ	γ	γ	γ	γ
d_{50} (μm)[a]	76	72	62	–	–	–	66	74	68	90	151	128

[a] d_{50} is the median particle diameter.

larger median particle diameter was obtained with seed loadings of 2% and 4% at high supersaturation.

The polymorphic and morphological outcomes of seeded cooling crystallization of IMC from ethanol under all of the experimental conditions investigated in this work are summarized in Table 4. It is evident that the crystallization process parameters do influence the particulate properties of IMC. The crystallization courses for all of the seeded cooling crystallization experiments are projected on the solubility diagram of IMC polymorphs as shown in Figure 13. It is evident that the supercooled solutions at high supersaturation at 5 and 15 °C (points 1 and 2, respectively) are supersaturated in terms of both the α-IMC and γ-IMC polymorphs. According to Ostwald's rule of stages, metastable α-IMC is expected to crystallize first in such situations, followed by the solvent-mediated transformation into more stable γ-IMC.[42] In the case of crystallization at 15 °C, addition of γ-IMC seeds altered the outcome, while it did not influence the outcome at 5 °C with high supersaturation. For crystallization experiments with low supersaturation at 5 and 15 °C (points 3 and 4, respectively), although a marginal supersaturation was achieved for α-IMC, addition of γ-IMC seeds dictated the outcome. The existence of a critical supersaturation between the two levels used in this work for crystallization of IMC at 5 °C, above which the presence of γ-IMC seeds does not dictate the outcome, is apparent from the results. The present work clearly establishes the fact that the outcome of a crystallization process can be engineered through careful crafting of the crystallization process parameters to produce APIs of consistent and desired quality.

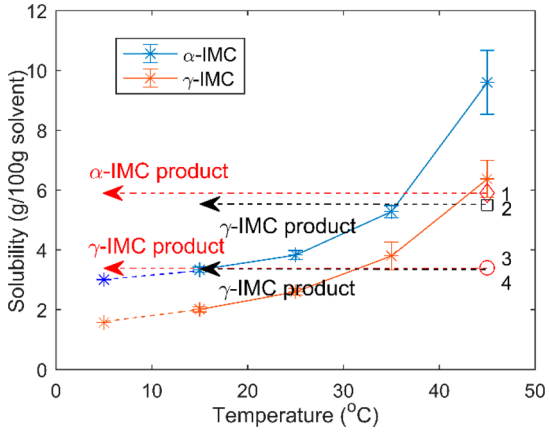

Figure 13. Projections of the crystallization course of IMC from ethanol on the solubility diagram. Points 1 and 3 denote high and low supersaturation at 5 °C, respectively; points 2 and 4 denote high and low supersaturation at 15 °C, respectively.

4. CONCLUSION

Solubility of γ-IMC was measured in different solvents at temperatures ranging from 15 to 45 °C with the aim of selecting crystallization solvents, followed by measurement of IMC induction times in the selected solvents. In order to establish the thermodynamic boundaries associated with the two polymorphs of IMC, the solubility of α-IMC was also measured in ethanol. The highest solubility of γ-IMC was observed in acetone, while lowest was in acetonitrile. Solid-phase analysis of excess solute during the solubility measurements confirmed the formation of solvates in acetone, methanol, and dichloromethane at all temperatures studied. Longer induction times of IMC were observed in ethanol, while shorter induction times were observed in acetone, from which the IMC−acetone solvate was nucleated. Metastable α-IMC was nucleated from ethanol, while no nucleation was observed

DOI: 10.1021/acs.oprd.8b00078
Org. Process Res. Dev. 2018, 22, 697−706

from ethyl acetate at the studied temperatures and supersaturations. Analysis of possible IMC−solvent non-covalent interactions suggests the role of hydrogen bonding and C−H···π interactions in delaying the nucleation from ethanol and inhibiting nucleation from ethyl acetate, respectively. Results of cooling crystallization of IMC from ethanol seeded with γ-IMC suggests that the supersaturation, temperature, and seed loading do influence the polymorphism and morphology of IMC. Thermodynamically stable γ-IMC crystals with a well-defined rhombic platelike shape were obtained in all of the experiments except at 5 °C with high supersaturation (4.8), where α-IMC crystals with fine needlelike shape were obtained. At 5 °C with high supersaturation, the crystallization of IMC follows the kinetically favored path leading to the crystallization of metastable α-IMC despite seeding with γ-IMC. In terms of crystal size distribution, larger-sized particles were obtained at 15 °C with high supersaturation (2.6). The bimodal distribution of crystal sizes obtained in all of the experiments was the result of seed crystal growth, secondary nucleation, breakage, or a combination of secondary nucleation and breakage. Thus, this work confirms the effect of operating parameters on the outcome of crystallization of IMC from ethanol in terms of polymorphism and morphology and highlights the importance of operating the crystallization process within the design space in order to obtain the desired outcome.

■ ASSOCIATED CONTENT

Supporting Information

The Supporting Information is available free of charge on the ACS Publications website at DOI: 10.1021/acs.oprd.8b00078.

FT-Raman spectra showing distinct features of carbonyl group vibrations in α- and γ-IMC, thermograms showing the melting points and melting enthalpies of α- and γ-IMC, a thermogram of the IMC−acetone solvate, and XRPD patterns of IMC−acetone and IMC−dichloromethane solvates (PDF)

■ AUTHOR INFORMATION

Corresponding Author

*E-mail: crm@kbm.sdu.dk. Phone: +45 65508669.

ORCID

Chandrakant R. Malwade: 0000-0002-6911-962X

Notes

The authors declare no competing financial interest.

■ ACKNOWLEDGMENTS

The authors thank the Danish Council for Independent Research (DFF) for financing this work through Grant DFF-6111-00077B.

■ REFERENCES

(1) Datta, S.; Grant, D. J. W. Crystal Structures of Drugs: Advances in Determination, Prediction and Engineering. *Nat. Rev. Drug Discovery* **2004**, *3* (1), 42−57.

(2) Bauer, J.; Spanton, S.; Henry, R.; Quick, J.; Dziki, W.; Porter, W.; Morris, J. Ritonavir: An Extraordinary Example of Conformational Polymorphism. *Pharm. Res.* **2001**, *18* (6), 859−866.

(3) Lee, A. Y.; Erdemir, D.; Myerson, A. S. Crystal Polymorphism in Chemical Process Development. *Annu. Rev. Chem. Biomol. Eng.* **2011**, *2* (1), 259−280.

(4) Bernstein, J. Controlling the Polymorphic Form Obtained. In *Polymorphism in Molecular Crystals*; Oxford University Press: Oxford, U.K., 2007; pp 66−93.

(5) Sun, C.; Grant, D. J. W. Influence of Crystal Shape on the Tableting Performance of L-Lysine Monohydrochloride Dihydrate. *J. Pharm. Sci.* **2001**, *90* (5), 569−579.

(6) Swaminathan, V.; Kildsig, D. O. The Effect of Particle Morphology on the Physical Stability of Pharmaceutical Powder Mixtures: The Effect of Surface Roughness of the Carrier on the Stability of Ordered Mixtures. *Drug Dev. Ind. Pharm.* **2000**, *26* (4), 365−373.

(7) Abu Bakar, M. R.; Nagy, Z. K.; Saleemi, A. N.; Rielly, C. D. The Impact of Direct Nucleation Control on Crystal Size Distribution in Pharmaceutical Crystallization Processes. *Cryst. Growth Des.* **2009**, *9* (3), 1378−1384.

(8) Braatz, R. D. Advanced Control of Crystallization Processes. *Annu. Rev. Control* **2002**, *26* (1), 87−99.

(9) Gao, Y.; Wang, J.; Wang, Y.; Yin, Q.; Glennon, B.; Zhong, J.; Ouyang, J.; Huang, X.; Hao, H. Crystallization Methods for Preparation of Nanocrystals for Drug Delivery System. *Curr. Pharm. Des.* **2015**, *21* (22), 3131−3139.

(10) Hansen, T. B.; Simone, E.; Nagy, Z.; Qu, H. Process Analytical Tools to Control Polymorphism and Particle Size in Batch Crystallization Processes. *Org. Process Res. Dev.* **2017**, *21* (6), 855−865.

(11) Hansen, T. B.; Taris, A.; Rong, B. G.; Grosso, M.; Qu, H. Polymorphic Behavior of Isonicotinamide in Cooling Crystallization from Various Solvents. *J. Cryst. Growth* **2016**, *450*, 81−90.

(12) Nicolaï, B.; Céolin, R.; Rietveld, I. B. Polymorphism and Solvation of Indomethacin. *J. Therm. Anal. Calorim.* **2010**, *102* (1), 211−216.

(13) Chen, X.; Morris, K. R.; Griesser, U. J.; Byrn, S. R.; Stowell, J. G. Reactivity Differences of Indomethacin Solid Forms with Ammonia Gas. *J. Am. Chem. Soc.* **2002**, *124* (50), 15012−15019.

(14) Slavin, P. A.; Sheen, D. B.; Shepherd, E. E. A.; Sherwood, J. N.; Feeder, N.; Docherty, R.; Milojevic, S. Morphological Evaluation of the Gamma-Polymorph of Indomethacin. *J. Cryst. Growth* **2002**, *237−239*, 300−305.

(15) Thakral, N. K.; Mohapatra, S.; Stephenson, G. A.; Suryanarayanan, R. Compression-Induced Crystallization of Amorphous Indomethacin in Tablets: Characterization of Spatial Heterogeneity by Two-Dimensional X-Ray Diffractometry. *Mol. Pharmaceutics* **2015**, *12* (1), 253−263.

(16) Aceves-Hernandez, J. M.; Nicolás-Vázquez, I.; Aceves, F. J.; Hinojosa-Torres, J.; Paz, M.; Castañ O, V. M. Indomethacin Polymorphs: Experimental and Conformational Analysis. *J. Pharm. Sci.* **2009**, *98* (7), 2448−2463.

(17) Lohani, S.; Nesmelova, I. V.; Suryanarayanan, R.; Grant, D. J. W. Spectroscopic Characterization of Molecular Aggregates in Solutions: Impact on Crystallization of Indomethacin Polymorphs from Acetonitrile and Ethanol. *Cryst. Growth Des.* **2011**, *11* (6), 2368−2378.

(18) Patel, D. D.; Joguparthi, V.; Wang, Z.; Anderson, B. D. Maintenance of Supersaturation I: Indomethacin Crystal Growth Kinetic Modeling Using an Online Second-Derivative Ultraviolet Spectroscopic Method. *J. Pharm. Sci.* **2011**, *100* (7), 2623−2641.

(19) Cox, P. J.; Manson, P. L. γ-Indomethacin at 120 K. *Acta Crystallogr., Sect. E: Struct. Rep. Online* **2003**, *59* (7), o986−o988.

(20) Kaneniwa, N.; Otsuka, M.; Hayashi, T. Physicochemical Characterization of Indomethacin Polymorphs and the Transformation Kinetics in Ethanol. *Chem. Pharm. Bull.* **1985**, *33* (8), 3447−3455.

(21) Taylor, L. S.; Zografi, G. Spectroscopic Characterization of Interactions between PVP and Indomethacin in Amorphous Molecular Dispersions. *Pharm. Res.* **1997**, *14* (12), 1691−1698.

(22) Atef, E.; Chauhan, H.; Prasad, D.; Kumari, D.; Pidgeon, C. Quantifying Solid-State Mixtures of Crystalline Indomethacin by Raman Spectroscopy Comparison with Thermal Analysis. *ISRN Chromatogr.* **2012**, *2012*, 1−6.

(23) Kistenmacher, T. J.; Marsh, R. E. Crystal and Molecular Structure of an Antiinflammatory Agent, Indomethacin, 1-(P-

Chlorobenzoyl)-5-Methoxy-2-Methylindole-3-Acetic Acid. *J. Am. Chem. Soc.* **1972**, *94* (4), 1340−1345.
(24) Malwade, C. R.; Christensen, L. P. Simple Multipurpose Apparatus for Solubility Measurement of Solid Solutes in Liquids. *Educ. Chem. Eng.* **2016**, *16*, 29−38.
(25) Brittain, H. G. Thermodynamic vs. Kinetic Solubility: Knowing Which is Which. http://www.americanpharmaceuticalreview.com/Featured-Articles/160452-Thermodynamic-vs-Kinetic-Solubility-Knowing-Which-is-Which/.
(26) Saal, C.; Petereit, A. C. Optimizing Solubility: Kinetic versus Thermodynamic Solubility Temptations and Risks. *Eur. J. Pharm. Sci.* **2012**, *47* (3), 589−595.
(27) Togkalidou, T.; Fujiwara, M.; Patel, S.; Braatz, R. D. Solute Concentration Prediction Using Chemometrics and ATR-FTIR Spectroscopy. *J. Cryst. Growth* **2001**, *231* (4), 534−543.
(28) Kadam, S. S.; Mesbah, A.; van der Windt, E.; Kramer, H. J. M. Rapid Online Calibration for ATR-FTIR Spectroscopy during Batch Crystallization of Ammonium Sulphate in a Semi-Industrial Scale Crystallizer. *Chem. Eng. Res. Des.* **2011**, *89* (7), 995−1005.
(29) Hellstén, S.; Qu, H.; Louhi-Kultanen, M. Screening of Binary Solvent Mixtures and Solvate Formation of Indomethacin. *Chem. Eng. Technol.* **2011**, *34* (10), 1667−1674.
(30) Davey, R. J.; Schroeder, S. L. M.; Ter Horst, J. H. Nucleation of Organic Crystals—A Molecular Perspective. *Angew. Chem., Int. Ed.* **2013**, *52* (8), 2166−2179.
(31) Sanz, A.; Jiménez-Ruiz, M.; Nogales, A.; Martín y Marero, D.; Ezquerra, T. A. Hydrogen-Bond Network Breakage as a First Step to Isopropanol Crystallization. *Phys. Rev. Lett.* **2004**, *93* (1), 015503.
(32) Davey, R. J.; Dent, G.; Mughal, R. K.; Parveen, S. Concerning the Relationship between Structural and Growth Synthons in Crystal Nucleation: Solution and Crystal Chemistry of Carboxylic Acids as Revealed through IR Spectroscopy. *Cryst. Growth Des.* **2006**, *6* (8), 1788−1796.
(33) Robertson, C. C.; Wright, J. S.; Carrington, E. J.; Perutz, R. N.; Hunter, C. A.; Brammer, L. Hydrogen Bonding vs. Halogen Bonding: The Solvent Decides. *Chem. Sci.* **2017**, *8* (8), 5392−5398.
(34) Tulashie, S. K.; Lorenz, H.; Malwade, C. R.; Seidel-Morgenstern, A. Ternary Solubility Phase Diagrams of Mandelic Acid and N -Methylephedrine in Chiral Solvents with Different Carbon Chain Lengths. *Cryst. Growth Des.* **2010**, *10* (9), 4023−4029.
(35) Kojić-Prodić, B.; Štefanić, Z.; Žinić, M. Hydrogen Bonding and Molecular Assemblies. *Croat. Chem. Acta* **2004**, *77* (3), 415−425.
(36) Cui, P.; Zhang, X.; Yin, Q.; Gong, J. Evidence of Hydrogen-Bond Formation during Crystallization of Cefodizime Sodium from Induction-Time Measurements and in Situ Raman Spectroscopy. *Ind. Eng. Chem. Res.* **2012**, *51* (42), 13663−13669.
(37) Nishio, M.; Umezawa, Y.; Suezawa, H.; Tsuboyama, S. The CH/π Hydrogen Bond: Implication in Crystal Engineering. In *The Importance of Pi-Interactions in Crystal Engineering*; Tiekink, E. R. T., Zukerman-Schpector, J., Eds.; Frontiers in Crystal Engineering; John Wiley & Sons: Chichester, U.K., 2012; pp 1−39.
(38) Bishop, R. New Aspects of Aromatic $\pi\cdots\pi$ and CH$\cdots\pi$ Interactions in Crystal Engineering. In *The Importance of Pi-Interactions in Crystal Engineering: Frontiers in Crystal Engineering*; Tiekink, E. R. T., Zukerman-Schpector, J., Eds.; John Wiley & Sons: Chichester, U.K., 2012; pp 41−77.
(39) Desiraju, G. R. Cryptic Crystallography. *Nat. Mater.* **2002**, *1* (2), 77−79.
(40) Karthick, N. K.; Kumbharkhane, A. C.; Joshi, Y. S.; Mahendraprabu, A.; Shanmugam, R.; Elangovan, A.; Arivazhagan, G. Molecular Interactions in Ethyl Acetate-Chlorobenzene Binary Solution: Dielectric, Spectroscopic Studies and Quantum Chemical Calculations. *Spectrochim. Acta, Part A* **2017**, *178*, 218−224.
(41) Tian, F.; Qu, H.; Louhi-Kultanen, M.; Rantanen, J. Mechanistic Insight into the Evaporative Crystallization of Two Polymorphs of Nitrofurantoin Monohydrate. *J. Cryst. Growth* **2009**, *311* (8), 2580−2589.
(42) Davey, R. J.; Allen, K.; Blagden, N.; Cross, W. I.; Lieberman, H. F.; Quayle, M. J.; Righini, S.; Seton, L.; Tiddy, G. J. T. Crystal Engineering − Nucleation, the Key Step. *CrystEngComm* **2002**, *4* (47), 257−264.

DOI: 10.1021/acs.oprd.8b00078
Org. Process Res. Dev. 2018, 22, 697−706